Pearl farming micro-nanoplastics affect both oyster physiology and pearl quality

Tony Gardon (tony.gardon@ifremer.fr)
Ifremer
Jérémy Le Luyer
Université Laval https://orcid.org/0000-0001-9409-3196
Gilles Le Moullac
French Research Institute for Exploitation of the Sea
Claude Soyez
Ifremer
Fabienne Lagarde
IMMM
Alexandre Dehaut
ANSES
Ika Paul-Pont
CNRS
Arnaud Huvet
Institut français de recherche pour l'exploitation de la mer https://orcid.org/0000-0001-6912-881X

Article

Keywords:

Posted Date: July 6th, 2023

DOI: https://doi.org/10.21203/rs.3.rs-3127557/v1

Abstract

The widespread contamination of pearl farming lagoons in French Polynesia by microplastics has led to questions about risks for the pearl industry. The aim of this study was to test the effects of micro-nanoplastics (MNPs) on the pearl oyster (*Pinctada margaritifera*) over a 5-month pearl production cycle. MNPs were produced from plastic pearl farming gear and used at a concentration that oysters may encounter in lagoons. MNP exposure led to the alteration of energy metabolism, mostly driven by a lower assimilation efficiency of microalgae, with modulation of gene expression patterns. Pearl biomineralization was impacted by thinner aragonite crystals, with harvest marked by the presence of abnormal biomineral concretions, called keshi pearls. These experimental results demonstrated that MNPs threaten pearl oyster biology, with potential detrimental effects on pearl quality. Ecological approaches are now required to test the holistic impact of MNPs on population sustainability in the Polynesian pearl industry.

Introduction

Increasing amounts of plastic debris in the environment are a global concern. As plastic production and global consumption outpace proper waste management, plastic waste is accumulating in the environment; this plastic increasingly ends up in the ocean[1]. Plastic debris can remain in the marine environment for many years due to slow degradability[2]. Owing to a combination of environmental factors (*e.g.*, ultraviolet radiation, physical forces and hydrolysis)[3], large plastic debris can break down into smaller fragments, 92% of which are plastic microparticles called "microplastics" (MPs, defined as plastic particles < 5 mm)[4]. Given their ubiquitous nature and small size, MPs have emerged as a global issue, leading to increased concerns about their ecological impacts[5]. MPs are likely to be ingested by a wide range of organisms[6], as demonstrated under laboratory conditions in filter-feeding species[7,8] and based on MP contamination of digestive tracts in wild animals[9,10]. Experimental consumption of MP can result in adverse health impacts, including both physical (*e.g.*, obstruction of the digestive tract) and chemical effects (*e.g.*, endocrine disruption) affecting biological functions such as respiration[11], nutrition[12], assimilation efficiency[8], reproduction[7] and growth[13]. However, laboratory experiments have mostly used a single polymer type that was usually spherical in shape (called model particles) at concentrations often higher in terms of the number of particles per volume than those found in the field[14,15]. However, the actual environmental exposure to MPs is more complex, involving various particle shapes, sizes, polymer types, surface characteristics and chemical compositions, which highlights the complexity of studying the actual ecological impact of MPs in aquatic ecosystems[15,16]. Although a few studies have tried to consider the complexity of *in situ* MP exposure[17–19], the gap between potential risks and actual risks associated with MP remains large[15,20].

In French Polynesia (FP), pearl farming is the second most important economic resource ($22.3 M in 2020), with the trade of pearl and mother-of-pearl being widespread in 28 island and atoll lagoons[21]. However, pearl farming is associated with a specific source of plastics since most gear (*e.g.*, ropes,

collectors, and buoys) is made of synthetic materials that accumulate over time and represent potential hotspots of MP release[22]. A recent monitoring study in pearl farming lagoons revealed widespread MP contamination in seawater and cultured pearl oysters[23]. The water column was demonstrated to be a highly contaminated compartment (from 14 to 716 MP m^{-3}); pearl oysters are cultivated in this compartment and therefore subject to substantial microscale MP pollution (2–125 MP g^{-1} dry weight)[23]. Ropes and spat collectors, the main types of plastic gear used in pearl farming, which are both made of polyethylene (PE) and polypropylene (PP), were suggested as the main contributors to the dominant small-sized (20–200 µm) and fragment-shaped MPs[23]. Hence, pearl farming could be the origin of its own plastic pollution risk, with potential impacts on the pearl oyster, *Pinctada margaritifera*, and more broadly on marine life and lagoon ecosystems.

Experimental exposure involving polystyrene microbeads has already demonstrated a dose-dependent effect on energy balance[8] and dose-specific transcriptomic disruption of gene expression[24] in *P. margaritifera*. In the present study, a more realistic scenario was tested using chronic exposure of pearl oysters to pearl farming micro-nanoplastics (MNPs) over a 5-month pearl production cycle and considering important endpoints such as pearl quality. Three different MNP concentrations were used: 0 (control), 0.025 and 1 µg L^{-1} (both included in the range of 0.003–3 µg L^{-1} extrapolated from *in situ* data point of 716 MP m^{-3} for a particle size range of 20–200 µm). An integrative approach was used to assess the effects of this exposure at the individual, cellular and molecular levels. Special attention has been given to pearl production, including pearl formation and quality as well as biomineralization processes. Demonstrating effects in a more realistic scenario should support decision-making, changes in industry processes and legislation outlining government policies to limit this emerging risk to lagoon ecosystems and pearl farming sustainability.

Results

Metabolic rates

MNP exposure led to a significantly higher ingestion rate in oysters exposed to 1 µg L^{-1} ($12.4 \pm 0.6 \times 10^7$ cells h^{-1} g^{-1}) than in oysters exposed to the control ($10.7 \pm 0.5 \times 10^7$ cells h^{-1} g^{-1}) and 0.025 µg L^{-1} ($10.5 \pm 0.6 \times 10^7$ cells h^{-1} g^{-1}) conditions (Tukey's HSD, $P < 0.001$) (Fig. 1b). Furthermore, a significantly lower assimilation efficiency was observed in oysters exposed to 1 µg L^{-1} (26.1 ± 5.2%) than in control oysters (37.5 ± 3.4%; Tukey's HSD, $P < 0.001$), while only a downward trend was observed in oysters in the 0.025 µg L^{-1} condition (31.4 ± 3.3%; Tukey's HSD, $P = 0.100$) (Fig. 1d). No significant difference was observed regarding oxygen consumption (ANOVA, $P = 0.420$), with a mean of 0.79 ± 0.08, 0.81 ± 0.07 and 0.85 ± 0.06 mg O_2 h^{-1} g^{-1} under control, 0.025 µg L^{-1} and 1 µg L^{-1} conditions, respectively (Fig. 1c).

Scope for growth

Metabolic rate analysis revealed a mean energy balance (scope for growth) of 31.2 ± 3.9, 22.2 ± 4.7 and 22.6 ± 6.8 J h^{-1} g^{-1} for the control, 0.025 µg L^{-1} MNP and 1 µg L^{-1} MNP conditions, respectively (Fig. 1e). The overall Kruskal–Wallis (KW) test was at the limit of significance (P = 0.050), and multiple comparisons revealed a slight significant difference in means between the control and 0.025 µg L^{-1} conditions (Dunn's test, P = 0.048) (Fig. 1e).

Energy reserve

The glycogen content analysis on pearl oyster muscle revealed a significantly lower energy reserve in the 0.025 µg L^{-1} (4.6 ± 0.8 µg mg^{-1}) condition compared with the control (8.1 ± 1.2 µg mg^{-1}) and 1 µg L^{-1} (7.9 ± 1.5 µg mg^{-1}) conditions (Tukey's HSD test, P < 0.001 and P = 0.001, respectively) (Fig. 1f).

Gametogenesis

All pearl oysters were of the male sex, except one individual of the female sex in the control condition. No sign of abnormal gametogenesis was observed by gonad cross-section histology analysis, regardless of condition.

Shell growth

No significant difference in shell growth was observed among conditions (ANOVA, P = 0.321), as suggested by the similar shell deposit rate between conditions, with values of 5.1 ± 0.5 µm day^{-1} in the control, 5.1 ± 0.6 µm day^{-1} in the 0.025 µg L^{-1} condition and 5.6 ± 0.5 µm day^{-1} in the 1 µg L^{-1} condition) (Fig. 1g).

Pearl rotation

The mean angular speed of pearl rotation in the pearl sac of *P. margaritifera* was similar among conditions (ANOVA, P = 0.355), with values of 5.9 ± 2.6, 4.0 ± 1.5 and 6.5 ± 1.3 deg min^{-1} in the control, 0.025 and 1 µg L^{-1} conditions, respectively.

Harvest

The number of pearls collected at the end of the experiment was statistically similar among conditions in terms of frequency distribution (χ^2 = 0.164, P = 0.921), with a mean of 62.4 ± 12.8% (N = 23) for individuals that produced pearls in the control condition, 59.7 ± 17.4% (N = 27) for individuals that produced pearls in the 0.025 µg L^{-1} condition and 59.9 ± 11.4% (N = 31) for individuals that produced pearls in the 1 µg L^{-1} condition (Fig. 2a and b). However, a significant difference in the frequency distribution of the production of keshi pearls, *i.e.* pearl oysters that have rejected their nucleus (Fig. 2a and c), was observed between the control and 1 µg L^{-1} conditions (Fisher's exact test, P = 0.039); the

0.025 µg L^{-1} condition had an intermediate value that was not significantly different (Fisher's exact test, $P = 0.144$). Indeed, a mean of 9.9 ± 8.3% ($N = 4$) and 17.6 ± 9.1% ($N = 9$) of pearl oysters produced keshi pearls in the 0.025 and 1 µg L^{-1} conditions, respectively, while no keshi pearls were collected in the control condition ($N = 0$; Fig. 2a).

Pearl quality traits

Pearl nacre deposition measured on the nucleus and composed of periostracum, calcite and aragonite crystals (Fig. 2d) reached similar mean values of 80.2 ± 12.2 µg in the control condition, 85.4 ± 17.8 µg in the 0.025 µg L^{-1} condition, and 78.0 ± 21.1 µg in the 1 µg L^{-1} condition (KW test, $P = 0.717$). Similarly, no significant difference in biomineralization rate (thickness) was measured among conditions (ANOVA, $P = 0.430$), with values of 3.0 ± 0.5, 3.4 ± 0.7 and 2.9 ± 0.6 µm d^{-1} in the control, 0.025 and 1 µg L^{-1} conditions, respectively (Fig. 2e). However, a significantly higher proportion of organic material in the coating on the nucleus (periostracum) was measured in the 0.025 µg L^{-1} condition (7.3 ± 6.5%) compared to the control (1.2 ± 1.9%) (Dunn's test, $P = 0.025$), while no difference was observed regarding calcite and aragonite crystals (KW test, $P = 0.258$ and $P = 0.148$, respectively) (Fig. 2f). Focusing on aragonite crystals at the microstructure level, no significant difference in aragonite front spacing (Fig. 2g and h) was measured on the pearl surface (KW test, $P = 0.950$), with a mean of 16.3 ± 1.9 µm in the control condition, 15.9 ± 1.7 µm in the 0.025 µg L^{-1} condition and 18.2 ± 3.9 µm in the 1 µg L^{-1} condition (Fig. 2g). However, a significant difference in aragonite platelet thickness (Fig. 2i and j) was measured (KW test, $P = 0.010$), with values of 491.9 ± 45.3, 442.4 ± 36.1 and 395.1 ± 18.5 nm in the control, 0.025 and 1 µg L^{-1} conditions, respectively, revealing a significantly lower value in the 1 µg L^{-1} condition compared to the control condition (Dunn's test, $P = 0.002$; Fig. 2i).

Keshi pearl origin

First, keshi pearl observation with a stereomicroscope led to the visualization of a purple particle (~ 9 µm), the typical color of the synthetic rope, embedded in the mineral surface microlayer of a keshi pearl produced by a pearl oyster exposed to 1 µg L^{-1} MNPs (Fig. 2k and l). After a soft sanding step, the particle was tentatively identified using µ-Raman but remained embedded in a thin mineral layer and was lost during additional soft sanding. This approach thus failed to identify a PE signature corresponding to the MNP produced from weathered purple synthetic rope (Fig. 2m and n). To overcome losses due to sanding, the particles were first tentatively analyzed as a whole by Py-GC—MS, but the MS signals were not workable. In a second attempt, a keshi pearl was dissolved with 98% sulfuric acid after confirming the innocuousness of this chemical for both PE and PP fragments. With this approach, some black fragments were observed and tentatively identified using µFT-IR, but none of them matched the signature of spat collectors (PP).

RNA-Seq data

RNA sequencing of mantle ($N = 29$), hemocyte ($N = 29$) and pearl sac ($N = 29$) samples yielded means of 36.6 ± 4.5, 33.2 ± 3.3 and 34.4 ± 2.3 M raw reads per individual, respectively. After trimming, 95.2% of

reads were recovered in mantle, hemocyte and pearl sac samples and used for downstream analyses. The mapping rate reached 46.0 ± 1.1%, 36.1 ± 0.8% and 42.2 ± 1.0% in mantle, hemocyte and pearl sac samples, respectively, with no significant differences among conditions (ANOVA, $P = 0.609$, $P = 0.149$ and $P = 0.191$, respectively). Sequencing results and read survival after trimming and mapping are shown in Supplementary Table 1.

Global gene expression patterns across tissues and conditions

Patterns of up- and downregulation within euKaryotic Orthologous Groups (KOG) classes were used to compare MNP conditions with global gene expression data generated from mantle, hemocytes and pearl sac of *P. margaritifera* in response to 0 (control), 0.025 and 1 µg MNPs L^{-1}. A hierarchical clustering analysis comparing the change in magnitude and direction of gene expression within each KOG class among datasets revealed that the patterns of the 0.025 and 1 µg L^{-1} conditions were mostly similar (Fig. 3a-c) but that largely differences occurred across tissues. Indeed, *P. margaritifera* KOG functional enrichment correlated across conditions and tissues, with Pearson's r values of 0.74 ($P < 0.001$), 0.90 ($P < 0.001$) and 0.56 ($P = 0.004$) for the mantle, hemocytes and pearl sac, respectively (Fig. 3a-c). No significant correlations in gene expression were detected among tissue samples from each MNP condition, except between mantle and pearl sac datasets for the 1 µg L^{-1} condition ($r = 0.59$, $P = 0.002$) (Supplementary Fig. 1).

In the mantle, individuals exposed to MNPs exhibited upregulation of genes involved in "energy production and conversion" (0.025 and 1 µg L^{-1}, $P_{adj} < 0.001$), which was the most significant enrichment, followed by "replication, recombination and repair" (0.025 µg L^{-1} MNPs, $P_{adj} = 0.049$; 1 µg L^{-1} MNPs, $P_{adj} = 0.016$). Regarding downregulated genes, the most significant enrichment common to both MNP conditions was associated with "cytoskeleton" (0.025 and 1 µg L^{-1}, $P_{adj} < 0.001$), although this KOG class was upregulated in hemocyte samples, followed by "signal transduction mechanisms" (0.025 and 1 µg L^{-1} MNPs, $P_{adj} < 0.001$, respectively) (Fig. 3d). Hemocytes of exposed oysters also exhibited downregulation of genes associated with "nuclear structure" (0.025 µg L^{-1} MNPs, $P_{adj} = 0.047$; 1 µg L^{-1} MNPs, $P_{adj} < 0.001$), "RNA processing and modification" and "translation, ribosomal structure and biogenesis" (0.025 and 1 µg L^{-1} MNPs, $P_{adj} < 0.001$, respectively) (Fig. 3d). Finally, in the pearl sac, individuals exposed to MNP conditions exhibited common enrichment of upregulated genes involved in "chromatin structure and dynamics" (0.025 µg L^{-1} MNPs, $P_{adj} = 0.009$; 1 µg L^{-1} MNPs, $P_{adj} = 0.031$) (Fig. 3d). Some unique patterns specific to MNP conditions were also observed, as shown in Fig. 3d.

Gene coexpression modules associated with MNPs and physiological traits

Mantle module functional enrichment

The expression values of 23,610 genes in 29 mantle samples were used to construct the coexpression module by weighted gene coexpression network analysis (WGCNA). Overall, 26 module genes were detected and labeled with different colors (Supplementary Fig. 2). After clustering of module eigengenes (MEs) based on dissimilarity, a total of 10 modules were selected according to module-trait relationships ($r \geq 0.45$, $P \leq 0.01$) regarding correlations of ME expression with experimental conditions and physiological traits (Fig. 4a and Supplementary Fig. 3). Among the modules of interest, 5 modules (cluster 1) were characterized by reduced expression under MNP conditions compared to control conditions, with the darkgrey ($N = 103$ genes) and turquoise ($N = 5,346$ genes) modules showing significantly lower ME expression at 0.025 (Dunn's test, $P = 0.043$) and 1 (Dunn's test, $P = 0.023$) µg L^{-1} MNPs, respectively (Fig. 4b). In the darkgrey module, gene ontology (GO) enrichment analysis of biological process (BP) highlighted "negative regulation of calcium ion-dependent exocytosis" (GO:0045955, $P_{adj} < 0.001$). The turquoise module exhibited several representative enrichments ($N = 15$ GO) associated with cell organization and biogenesis, metabolism, development and signal transduction (Fig. 4c). Four modules were also identified in cluster 2, with the brown module ($N = 1,606$ genes) showing significantly higher ME expression at 1 µg L^{-1} MNPs than under the control conditions (Tukey's HSD test, $P = 0.006$). The most significant enrichments identified in this module were "chitin metabolic process" (GO:0006030, $P_{adj} < 0.001$), "positive regulation of lipoprotein transport" (GO:0140077, $P_{adj} < 0.001$), "ribonucleoside catabolic process" (GO:0042454, $P_{adj} = 0.006$) and "biological adhesion" (GO:0022610, $P_{adj} = 0.005$). Finally, the tan module ($N = 718$ genes; cluster 3) was identified as a key module showing a strong correlation with condition ($r = 0.67$, $P < 0.001$), specifically with 1 µg L^{-1} MNPs ($r = 0.69$, $P < 0.001$), and strong correlations with physiological traits such as ingestion ($r = 0.54$, $P = 0.002$) and assimilation ($r = -0.45$, $P = 0.01$) (Fig. 4a). This module exhibited significantly higher ME expression in the 1 µg L^{-1} group than in both the control and 0.025 µg L^{-1} groups (Dunn's test, $P = 0.007$ and $P = 0.014$, respectively) (Fig. 4b). The tan module was significantly enriched for "MAPK cascade" (GO:0000165, $P_{adj} < 0.001$), "omega-hydroxylase P450 pathway" (GO:0097267, $P_{adj} = 0.008$), "response to potassium ion" (GO:0035864, $P_{adj} < 0.001$) and "inorganic anion transport" (GO:0015698, $P_{adj} = 0.006$) (Fig. 4c). Details for all GO enrichments in BP and molecular function (MF) are provided for modules of interest in Supplementary Table 2.

Regarding the differentially expressed genes (DEGs) between the MNP conditions and the control conditions, a total of 438 DEGs were identified, with 88 DEGs *vs.* 0.025 µg L^{-1} MNPs and 405 DEGs *vs.* 1 µg L^{-1} MNPs; of these DEGs, 55 were common to both MNP conditions (Fig. 4d). A total of 24 and 64 up- and downregulated genes were found, respectively, from individuals treated under the 0.025 µg L^{-1} condition compared with the control and 246 and 159 up- and downregulated genes, respectively, from individuals treated under the 1 µg L^{-1} condition (Supplementary Fig. 7). Focusing on the tan module, a total of 82 DEGs (7 and 82 DEGs from 0.025 and 1 µg L^{-1} MNPs, respectively) were identified among the module genes, with 53 genes annotated according to UniProt entries (Supplementary Table 4). All DEGs were upregulated, and 7 DEGs were common to both MNP conditions, of which 6 were annotated (Fig. 4e and Supplementary Table 4). Furthermore, by focusing on shared DEGs among sample types ($N = 5$

DEGs; Fig. 5), a total of 4 DEGs were identified in the tan module (Fig. 4e and Supplementary Table 4), namely, *CYP2C8, CYP2J2* (cytochrome P450 transcripts), *HR4* (hormone receptor 4), and *SULT1B1* (sulfotransferase family 1B member 1), as being specific to the 1 µg L^{-1} condition (Fig. 5). A complete list of DEG distribution among WGCNA modules in mantle samples is available in Supplementary Table 4.

Hemocyte module functional enrichment

A coexpression module was constructed by WGCNA of the expression values of 24,910 genes in 29 hemocyte samples. Overall, 12 modules were detected (Supplementary Fig. 4), and a total of 3 modules of interest were selected according to module-trait relationships ($r \geq 0.45$, $P \leq 0.01$), with 727, 1,020 and 2,092 genes in the magenta, pink and red modules, respectively (Supplementary Fig. 5). Among these 3 modules, none were related to condition, but the magenta module exhibited a strong correlation with 0.025 µg L^{-1} MNPs ($r = -0.67$, $P < 0.001$) and 1 µg L^{-1} MNPs ($r = -0.52$, $P = 0.004$), and there was a significant difference in ME expression between the control condition and both 0.025 and 1 µg L^{-1} conditions (Tukey's HSD test, $P = 0.022$ and $P = 0.017$, respectively) (Supplementary Fig. 5). This module was significantly enriched for "maturation of LSU-rRNA from tricistronic rRNA transcript" (GO:0002108, $P_{adj} < 0.001$), "cytoplasmic translation" (GO:0002181, $P_{adj} < 0.001$), "ribosomal small subunit assembly" (GO:0000028, $P_{adj} < 0.001$) and "establishment of protein localization to endoplasmic reticulum" (GO:0072599, $P_{adj} = 0.006$). Details for all GO enrichments in BP and MF are provided for the magenta, pink and red modules in Supplementary Table 3.

A total of 204 DEGs were identified under MNP conditions compared to the control conditions, with 132 DEGs *vs.* 0.025 µg L^{-1} MNPs and 110 DEGs *vs.* 1 µg L^{-1} MNPs, of which 38 were common DEGs (Supplementary Fig. 5). A total of 73 and 59 up- and downregulated genes, respectively, were found in individuals under the 0.025 µg L^{-1} condition compared with the control condition, and 55 and 55 up- and downregulated genes, respectively, in the 1 µg L^{-1} condition compared to the control condition (Supplementary Fig. 7). A complete list of DEG distribution among WGCNA modules in hemocyte samples is available in Supplementary Table 5.

Pearl sac module functional enrichment

A coexpression module was constructed by WGCNA of the expression values of 28,116 genes in 29 pearl sac samples. Overall, 11 modules were detected (Supplementary Fig. 6), but no modules were selected according to module-trait relationships ($r \geq 0.45$, $P \leq 0.01$).

A total of 146 DEGs were identified in MNP conditions compared to the control condition, with 80 DEGs *vs.* 0.025 µg L^{-1} MNPs and 73 DEGs *vs.* 1 µg L^{-1} MNPs, with 7 common DEGs. We found a total of 22 and 58 up- and downregulated genes, respectively, in individuals treated under the 0.025 µg L^{-1} condition compared with individuals treated under the control condition and 44 and 29 up- and downregulated genes, respectively, in the 1 µg L^{-1} condition (Supplementary Fig. 6). A complete list of DEGs in the pearl sac is available in Supplementary Table 6.

Discussion

Biochemical and physiological processes involved in the life cycle of heterotrophic organisms are closely dependent on (*i*) their ability to extract the necessary energy from their living environment *via* food intake and (*ii*) all the processes ensuring the management of energy at different levels of biological organization. The results of this study show that experimental MNP exposure, at concentrations equivalent to *in situ* MP mass concentrations, alters pearl oyster energy metabolism, with consequences at the individual, cellular and molecular levels, as well as disruption of harvest and pearl quality traits at the functional level.

The SFG defines the need for energy for growth beyond that required for maintenance and can thus be seen as a measure of an individual's potential to thrive in his or her environment. It is mainly driven by ingestion and assimilation efficiency[25], which influence energy gain in bivalves[26]. Here, the linear decrease in assimilation efficiency observed in individuals exposed to MNPs at a significantly lower level of 1 µg L^{-1} means that for an equal volume of water filtered by the oysters, the assimilation of microalgae was modified by the presence of MNPs. The energy provided by food intake was thus lower for exposed oysters, resulting in a slightly lower SFG, which was significant for the 0.025 µg L^{-1} condition. Although it was not sufficient to counterbalance energy loss, the ingestion rate was significantly higher in pearl oysters exposed to 1 µg L^{-1} MNPs than in those exposed to 0.025 µg L^{-1} MNPs, suggesting a compensatory effect. Indeed, increasing food intake to limit energetic loss was previously observed in the Pacific oyster after a 2-month exposure to polystyrene microbeads (micro-PS)[7]. The energy cost was not offset by the increase in oxygen consumption, which was similar among the three conditions; thus, the body may be forced to sacrifice some of the energy normally allocated to functions such as growth and/or reproduction[27]. Effects were not visible on the shell deposit rate, a proxy of growth, nor on gametogenesis. However, the low glycogen stores of pearl oysters exposed to 0.025 µg L^{-1} MNPs compared to the control condition (–3.5 µg mg^{-1}) and 1 µg L^{-1} MNPs (–3.3 µg mg^{-1}) may explain how individuals obtained their required energy.

Metabolic compensation during moderate stress exposure often involves elevated protein turnover and an associated increase in basal maintenance costs to cover the energy cost of stress protein expression and/or protein degradation pathways[27]. Our integrative approach including molecular responses demonstrated how stress response expression patterns can be both divergent and highly conserved among MNP concentrations. Indeed, the broad similarities in gene expression patterns among tissues of *P. margaritifera* exposed to 0.025 and 1 µg L^{-1} MNPs may reflect specific cellular stress responses to MNPs. Among common patterns, the upregulation of genes involved in "energy production and conversion" observed in the mantle illustrates the bioenergetic disorder that the oysters face and is hypothesized to be a general mechanism for protecting cells from oxidative stress[28]. A gene coexpression network revealed a module (the tan module, $N = 718$ genes) that appeared to be strongly correlated with experimental conditions and physiological traits. Among the genes of this module, upregulation of the mitogen-activated protein kinase (MAPK) cascade was the most representative

functional enrichment. MAPK pathways (the p38, JNK, and ERK signaling pathways) relay, amplify and integrate signals from a diverse range of stimuli and elicit appropriate physiological responses, including cellular proliferation, differentiation, development, inflammatory and stress responses, as well as apoptosis[29]. The activation of MAPK pathways was demonstrated to be triggered by reactive oxygen species (ROS) production in marine copepods exposed to micro-PS[30]. Moreover, this key module exhibited other representative functional enrichments that corroborate stress response mechanisms, such as response to potassium ions and the ω-hydroxylase P450 pathway. The activation of potassium channels, which are involved in the hydrolysis of ATP to generate energy, has been suggested to act as an early response to oxidative stress[31], while cytochrome P450 ω-hydroxylases play a fundamental role in the detoxification of xenobiotics and lipid metabolism[32]. Indeed, MPs are known to reduce lipid digestion by (*i*) decreasing the bioavailability of lipid droplets by forming large lipid-MP heteroaggregates and (*ii*) reducing lipase activity[33]. In this module, a diverse panel of lipid metabolism-related genes were identified as DEGs, such as *HDHD5*, common to both MNP conditions, and *CYP2C8* and *CYP2J2*, both identified in the mantle, hemocytes and pearl sac of oysters exposed to 1 µg L^{-1} MNPs. On the other hand, the five common DEGs identified in all tissues, which may reflect a conserved and specific response to MNPs, were associated with only the highest MNP concentration. This shows how stress response expression patterns can be divergent and/or dynamic on the basis of the role of energy homeostasis in setting limits to MNP stress tolerance. Some unique patterns were identified in the mantle, such as “carbohydrate transport and metabolism”, which was significantly enriched among upregulated genes in the 0.025 µg L^{-1} condition and may be linked with the low glycogen level measured in oyster muscle. A depletion of cellular energy stores (carbohydrates, lipids and proteins) has previously been demonstrated in mussels exposed to micro-PS[34]. The early depletion of glycogen is consistent with its role as a rapidly mobilizable metabolic fuel used to cover a rapid increase in energy demand in bivalves[34]. Thus, this immediate stress response is likely to precede the secondary cellular homeostasis response suggested in the 1 µg L^{-1} condition, involving a plethora of genes that act to reestablish homeostasis under the new environmental regime[35]. This is particularly true considering the discrepancy in the overall number of DEGs, which were nearly 5 times more abundant in the mantle of individuals exposed to 1 µg L^{-1} MNPs ($N = 405$) than individuals exposed to 0.025 µg L^{-1} MNPs ($N = 88$), reinforcing the existence of a dose-specific transcriptomic disruption of energy metabolism, as previously suggested[24]. The physiological and molecular signs observed in pearl oysters exposed to both MNP conditions are hallmarks of *pejus* conditions characterized by reduced fitness but positive growth and reproduction[27]. However, the more severe molecular disorders observed in the 1 µg L^{-1} condition seem to reflect a gradual transition of *P. margaritifera* from *pejus* to *pessimum* conditions, representing a high degree of stress[27]. Indeed, some unique patterns, such as “secondary metabolite biosynthesis, transport and catabolism”, that were enriched among upregulated genes in the 1 µg L^{-1} condition may illustrate an alteration in energy metabolism associated with defense mechanisms. Secondary metabolites (SMs) are generally produced to fulfill key functions involved in the interaction of the organism with its environment by modifying central metabolite precursors (*e.g.*, carbohydrates, lipids, and amino acids) to increase organismal

adaptation to environmental constraints[36]. Studies of the origins of animal SMs revealed that while some of them are made within the organism, the majority are diet-derived[37], especially through plant consumption[38]. SMs ingested by animals directly or *via* MPs after adsorption[39] can alter metabolic rates, reduce the digestibility of nutrients and compromise energy expenditure, depending on the type and amount of SM consumed[40]. In addition, the exploitation of SMs by animals has been demonstrated to be a strategy to protect against various challenges that perturb homeostasis due to their bioactive properties, such as antioxidants that protect against oxidative damage[40]. Further work is needed to understand the origin(s) of SMs and their role in *P. margaritifera* homeostasis by considering the interaction between microalgae-derived chemicals and MNPs, since this could be a key explanatory factor for the direct and indirect effects of MNPs on the living environment and biodiversity. Finally, *CYP2C8*, *CYP2J2* and *SULT1B1*, whose expression seems to be highly conserved in pearl oyster tissues exposed to 1 µg MNPs L^{-1}, are all related to the metapathway of biotransformation Phases I and II. Biotransformation is associated with chemical alteration of molecules such as nutrients, amino acids, toxins, and drugs in the body and should further be tested as biomarkers and potential environmental proxies to assess nutritional-MNP stress conditions of cultured pearl oysters and provide data to decision makers.

Pearl quality assessment revealed significant effects of MNP exposure on the microstructure of pearl nacre deposition, notably in aragonite crystals. Thinner aragonite platelets of pearls are known to be influenced by low temperature[41]. Ironically, this thin structure is more preferable to thicker aragonite platelets, at least in the latter phase of the culturing period, since aragonite platelets formed near the surface of the pearl just before harvest determine the pearl luster and interference color[41]. However, this effect occurred early only after a 3-month experimental cycle under MNP exposure, while the pearl production cycle proceeded for 18 months in nature. It is therefore conceivable that such an effect may be aggravated following prolonged/continuous MNP exposure, but such long-term alteration remains to be tested. Considering the influence of energy metabolism on shell growth[42] and its positive correlation with the pearl nacre deposition rate[43], the energy metabolism disruption observed in MNP-exposed pearl oysters may affect the pearl nacre deposition rate at the microstructural level. In the present study, the significant reduction in aragonite platelet thickness observed in the 1 µg L^{-1} condition is not consistent with the maintenance of a proper SFG through ingestion compensation. However, it is possible that this adaptation led to an altered pearl nacre microstructure rather than impairment of vital functions, considering the homeostasis disruption observed at the molecular level. Moreover, harvest at the end of the experiment demonstrated that pearl oysters that had rejected their nucleus post-grafting produced significantly more keshi pearls at 1 µg L^{-1} than oysters under the control condition in which keshi pearls were absent. MNPs may have induced keshi pearl production following possible translocation of MNPs across epithelial membranes[44] and/or external intrusion of MNPs through the incision made on the pearl pouch by the operator before receiver oyster healing. Indeed, small plastic particles can be embedded in shells during biomineralization[45]. While PE-PP particles were not identified within the mineral matrix of

keshi pearls, microscopy showed a particle of the expected size, shape and color, which is a distinct purple such as purple PE rope used for MNP production and exposure.

In conclusion, this study showed that mimicking the *in situ* conditions of MNP exposure can negatively affect different aspects of energy metabolism in *P. margaritifera*, interfering with energy assimilation and conversion and increasing energy costs for basal maintenance[27]. A compensatory effect on food intake was observed at a concentration of 1 µg L^{-1} MNPs, possibly to counterbalance the decrease in energy intake caused by digestive disruption of molecular functions involved in lipid metabolism; no such mechanism was observed at 0.025 µg L^{-1} MNPs, explaining the energy budget. It should therefore be noted that stronger impacts can be observed at lower doses, which is of great importance for understanding the effects of plastic pollution on ecosystems. Food availability is an aggravating factor for stress[46]. Considering the oligotrophic conditions of lagoon ecosystems, which are far from the nonlimiting food supply we experimentally applied here, stronger effects should be considered to occur under natural conditions. This is particularly true regarding the existence of multiple stressors, *i.e.*, temperature and acidification associated with global change, that could have a more profound impact on marine organisms when combined with MNP exposure[47]. This work highlights the risk of MNPs as part of the environmental exposure set (exposome) faced by pearl oysters and the related economy as well as lagoon ecosystems in French Polynesia.

Methods

Experimental animals

Pearl oysters were sampled on April 03, 2018, in a pearl farm located on Mangareva Island (23°06'34" S; 134°57'57" W) in the Gambier archipelago (23°07' S; 134°58' W, FP). A stock of 600 adult oysters (1.5–2 years old; height, 7.6 ± 0.6 cm; mean ± standard deviation) was transferred (transfer authorization No. 643 issued by the Ministry of Marine Resources of French Polynesia) to the lagoon of Vairao (Ifremer marine concession No. 8120/MLD: 17°48'26.0" S, 149°18'14.4" W, Tahiti, FP) on April 04, 2018. All the experimental procedures comply with French law and with institutional guidelines.

Pearl farming MNPs

MNPs were produced from two widely used types of pearl farming plastic gear (*i.e.*, synthetic rope and spat collectors), collected from weathered structures of a pearl farm in Manihi atoll (14°24'10.4" S, 145°57'29.2" W), according to the methodological protocol of Gardon et al.[48]. Based on FT-IR and Py-GC–MS measurements, the synthetic rope (SR) and spat collector (SC) were made of polyethylene (PE) and polypropylene (PP), respectively (Supplementary Fig. 8). These two polymers are the most commonly used plastic polymers worldwide and are often found in MPs sampled from pearl farming atolls[23]. The MNP size distribution ranged from 0.4 to 200 µm (Supplementary Fig. 9) following laser diffraction analysis (Beckman Coulter LS 130 particle laser diffractometer, Beckman Coulter, Inc., Brea, CA), matching the retention size range of *P. margaritifera* (*i.e.*, 2–200 µm)[49]. MNPs produced from SR and SC

were conserved separately in stock solutions, resuspended in filtered (1.2 µm) 70% ethanol at 1.5 g L^{-1} and stored at 4°C.

MNP exposure

A total of 240 pearl oysters (height, 7.6 ± 0.3 cm; weight, 36.1 ± 5.5 g) were conditioned in duplicate in 6 rectangular 500 L tanks (4 donors and 36 receivers for a total of 40 pearl oysters per tank, *i.e.*, 80 oysters per condition) at 26.5 ± 0.6°C (pH 8.2, dissolved oxygen 6.8 ± 0.5 mg O_2 L^{-1}, salinity 35 psu) under a 12 h light: 12 h dark cycle. The tanks were equipped with 2 air-lifts connected to the pressurized air circuit and 4 circulation pumps. A mixed diet of two microalgae (*Tisochrysis lutea* [*T-iso*] and *Chaetoceros gracilis*) was prepared daily in a cylindrical-conical 1000 L tank supplying continuous experimental tanks by a diaphragm pump at a dry-weight-algae/dry-weight-oyster ratio of 7–8% (*i.e.*, 35–40 cells $µl^{-1}$, below the threshold for triggering pseudofeces production). Before exposure, pearl oysters were placed in a 500 L tank for calcein marking performed at 150 mg L^{-1} (calcein diluted in seawater) overnight to assess the shell growth rate (see Supplementary Methods 1)[50].

After 2 weeks of acclimation, both types of MNPs (*i.e.*, SR and SC) were incorporated at equal weights and injected continuously at concentrations of 0 (control), 0.025 and 1 µg L^{-1}. The MNP concentrations tested in the present study were similar in terms of MP mass concentration to estimates from Gardon et al.[23] of concentrations that may occur in the pearl oyster living environment. Thus, the tested mass concentrations of 0.025 and 1 µg L^{-1} are both included in the range of *in situ* mass concentrations of 0.003–3 µg L^{-1} extrapolated from the numerical 20–200 µm MP concentration measured in the water column of the pearl farming atoll of Takaroa (*i.e.*, 716 MP m^{-3})[23]. Here, we tested 0.4–200 µm MNPs at 1 µg L^{-1}, and a 40-fold lower dose of 0.025 µg L^{-1} was therefore tested to get as close as possible to the "current" scenario (*i.e.*, number of particles per volume *vs.* mass concentration) as well as to target a response window for MNP stress based on previously reported dose-effects on oyster physiology[8] and gene expression[24]. The MNP mixture in 5 µm-filtered seawater was distributed continuously from a solution prepared daily in six cylindrical-conical 50 L tanks (1 per replicate). To limit aggregation, MNP solutions were added with Tween® 20 at a final concentration of 0.0002% (which is below the nontoxic concentration, 0.0007% v/v[51]) and distributed in all tanks, including the control.

Experimental grafts

After 2 months of exposure, pearl oysters were removed from the water for processing for the graft step. Receiver oysters were half-opened with a prop, and donor oysters were sacrificed. Ten mantle grafts from each donor were sampled and transplanted to receivers (1 donor for 10 receivers). For each receiver, one graft and one nucleus (2.0 BU size, Ø ~0.6 mm, ~ 0.4 g weight; Imai Seikaku Co. Ltd., Japan) were both inserted into the pearl pouch by a transplant specialist to simulate a pearl production cycle. Each nucleus was previously weighed with a highly accurate balance with ± 0.0001 mg accuracy to assess pearl nacre deposition on the surface after harvesting at the end of the exposure. One nucleus transplanted to one of

the 10 receivers per donor was a magnetized nucleus (*i.e.*, 4 per tank, 8 per treatment) for the assessment of pearl rotation in the pearl pouch (see Supplementary Methods 2)[52]. Once the receivers were grafted, all pearl oysters were put back in their respective experimental tanks to continue MNP exposure over a 3-month period.

Ecophysiological measurement

At 2 weeks post-graft (2.5 months exposure), ten receiver oysters per treatment were placed in an ecophysiological measurement system (EMS) to monitor the clearance rate and oxygen consumption. The EMS consisted of eleven hemispheric open-flow chambers in transparent Altuglas®. One oyster was placed in each chamber, and the eleventh chamber was occupied by an empty oyster shell to be used as a control[53]. Experimental conditions for *in vivo* exposure were replicated in the EMS during measurements. The flow rates in the chambers were constant at 12 L h^{-1}. Each chamber was equipped with a two-way electromagnetic valve activated by an automaton. The released water was analyzed for 3 min using a fluorometer (10-AUTM, Turner Designs, Sunnyvale, CA) to measure microalgae fluorescence and an oximeter (OXI 538/CellOX® 325, WTW, Weilheim, Germany) to measure dissolved oxygen. Data were recorded with acquisition software (computer programming by National Instruments™) for 3 min per chamber by alternating measurements in chambers with and without (control) oysters. Oysters remained in the chambers for at least 48 h; measurements of each oyster were taken every 24 min until 120 measurements of the clearance rate and oxygen consumption had been recorded[53]. A total of 120 pearl oysters were individually monitored in the EMS (40 oysters per treatment). Assimilation efficiency was measured after collecting feces in each hemispheric chamber and 50 ml of microalgae mixture administered during ecophysiological measurements[53].

Ingestion and respiration

The ingestion rate (IR) is an indicator of feeding activity[53] and is defined as the quantity of microalgae cleared per unit of time. IR was calculated as follows:

$$\mathrm{IR} = \mathrm{V} \times (\mathrm{C1} - \mathrm{C2})$$

1

where C1 is the fluorescence level of the control chamber, C2 is the fluorescence of the experimental chamber containing one oyster, and V is the constant water flow rate (12 L h^{-1})[53].

The oxygen consumption rate (OC) was measured (mg O_2 h^{-1}) by calculating the differences in OC between the control and experimental chambers:

$$\mathrm{OC} = \mathrm{V} \times (\mathrm{O1} - \mathrm{O2})$$

2

where O1 is the oxygen level in the control chamber, O2 is the oxygen level in the experimental chamber, and V is the water flow rate[53].

IR and OC were estimated, and an average was calculated for each oyster. The values were converted to a standard animal basis (1 g, dry weight) using the following formula:

$$\mathrm{Y}s = \left(\frac{\mathrm{W}s}{\mathrm{W}e}\right)^{b} \times \mathrm{Y}e$$

3

where Y*s* is the physiological activity of a standard oyster, W*s* is the dry weight of a standard oyster (1 g), W*e* is the dry weight of the specimen, Y*e* is the measured physiological activity, and *b* is the allometric coefficient of a given activity. The average *b* allometric coefficients were 0.66 for IR and 0.75 for OC[54].

Assimilation efficiency

The assimilation efficiency (AE) of organic matter was assessed by analyzing microalgae and feces according to the method of Conover (1966) and as described by Chávez-Villalba et al.[53]. Biodeposits of each individual were treated by filtration on a GF/C filter (1.2 µm porosity, Ø 47 mm) previously burned at 450°C and weighed. The filters were then dried at 60°C for 24 h to obtain the dry weight of biodeposits (DW) and then burned at 450°C for 4 h to obtain the weight of the mineral matter (W_{MM}). The weight of organic matter (W_{OM}) biodeposits is the difference between the DW and W_{MM}. The W_{OM} of the food ration was calculated by filtering 50 ml of the microalgae mixture, followed by treatment of biodeposits according to the procedure described for organic waste. After conversion of the W_{OM} biodeposits and W_{OM} microalgae to relative values, AE (%) was calculated as:

$$\mathrm{AE} = \frac{\mathrm{OM}m - \mathrm{OM}b}{(100 - \mathrm{OM}b) \times \mathrm{OM}m}$$

4

where AE is the assimilation efficiency, OM*m* (%) is the microalgae organic matter value (0.87 for *Tisochrysis lutea* and 0.6 for *Chaetoceros gracilis*) and OM*b* (%) is the waste organic matter (biodeposits).

Energy budget

Ecophysiology data were converted into energy values to define the scope for growth (SFG):

$$\mathrm{SFG} = (\mathrm{IR} \times \mathrm{AE}) - \mathrm{OC}$$

5

where IR is the ingestion rate, AE is the assimilation efficiency, and OC is the oxygen consumption. We used 20.3 J for 1 mg of particulate organic matter and 14.1 J for 1 mg O_2[55].

Oyster sampling

At the end of the 5-month exposure period, pearl oysters were dissected to collect, if present, pearls in pearl pouches or keshi pearls. When no pearl was present, nuclear rejection followed the graft step. Keshi pearl production sometimes occurs after rejection and corresponds to the biomineralization of the remaining grafted piece of mantle and/or particles that may penetrate the pearl pouch before healing of the transplantation incision. The visceral mass was then sampled, drained on absorbent paper and placed in 10% formalin seawater for 72 h before being transferred into 70% ethanol for histology analysis (see Supplementary Methods 3). A piece of mantle and a piece of pearl sac (in the case of pearl harvest) were also sampled from each pearl oyster, as well as hemocytes collected in the byssal gland with a needle (1 ml; 0.45 × 13 mm). These samples were placed in RNA later solution (500 µl) and stored at − 80°C before RNA extraction and sequencing for transcriptomic analysis. Each muscle from each pearl oyster was also sampled and frozen in liquid nitrogen before storage at − 80°C for energy reserve assessment by glycogen content (see Supplementary Methods 4).

Pearl quality trait measurements

The collected pearls were weighed with a balance with ± 0.0001 mg accuracy to measure the weight of pearl nacre deposited on the nucleus surface by subtracting the initial weight of the grafted nucleus. The pearls were then sawn into two equal parts with a “Swap Top” Trim Saw machine (Inland, Middlesex, UK), which included a diamond Trim Saw Blade (Thin Cut) IC-40961. One part was first fragmented into pieces using a hammer and screwdriver before 1 min of sonication in a 30% ethanol bath at 30 kHz to dissociate small particles from fragments. The fragments were then fixed with a carbon tab onto an aluminum stub (Ø 12.5 mm, Agar Scientific Ltd., UK) to analyze the mineralized portion of the nacre on the nucleus (S1), while the second part was directly fixed flat on another stub for pearl surface analysis (S2). The samples were metallized with a 15 nm layer of gold on their surface using a Rotary Pumped Coater (Quorum Technologies, Q150R ES model) and observed at 15 kV (in charge-up reduction mode) using a Hitachi TM 3030 scanning electron microscope (SEM). Images (300×) of fractured pearl (S1) were captured to measure the thickness of the periostracum (an organic coating on the nucleus), calcite and aragonite crystals. The biomineralization rate (*i.e.*, total thickness of the periostracum, calcite and aragonite crystals) was calculated by dividing the thickness of deposits by the time that had elapsed since grafting (expressed in µm d^{-1}). Focusing on the aragonite crystal microstructure, the thickness of platelets (S1) and the spacing of their organization into growth fronts on the pearl surface (S2) were measured ($1{,}064 \leq N \leq 2{,}454$ and $759 \leq N \leq 959$ per condition for S1 and S2, respectively) in high-magnification images (9,000× and 800×, respectively).

Keshi pearl analysis

For keshi pearls showing particles in the nacre layers under direct illumination on an Olympus SZX16 stereomicroscope equipped with a UC90 camera, the surface was soft sanded with very fine sandpapers (P1200 and Silicon Carbide 800/2400) usually used for sclerochronological studies. µRaman analyses

were carried out on a Horiba XploRA PLUS V1.2 following the procedure described by Hermabessiere et al.[56], and Py-GC–MS analyses were carried out on a Shimadzu QP2010-Plus device following the optimized method described in the same article. The analysis of whole keshi pearls was also carried out by dissolving the keshi pearls in 98% sulfuric acid and observing the remaining particles under a stereomicroscope. Some fragments collected after observation were also analyzed using a Perkin Elmer Spotlight™ 400 Fourier transform infrared (FT-IR) spectrometer equipped with an MCT detector coupled to a Spectrum 3 MIR spectrometer following the procedure described by Djouina et al.[57], except for the number of accumulations, which was set to 10 in the present study.

RNA extraction and sequencing

Total RNA was extracted from mantle, hemocyte and pearl sac samples with TRIZOL Reagent (Life Technologies, USA) at a ratio of 1 ml per 100 mg tissue, following the manufacturer's recommendations. RNA quantity and integrity were evaluated with a Nanodrop (NanoDrop Technologies Inc., USA) and a 2100 BioAnalyzer System (Agilent Technologies, USA). RNA was dried in RNA-stable solution (Thermo Fisher Scientific, USA) and shipped at ambient temperature to McGill sequencing platform services (Montreal, Canada). TruSeq RNA libraries were randomly multiplexed (N = 20 individuals per lane) and subjected to 100-bp paired-end sequencing on an Illumina NovaSeq 6000 system at the McGill Genome Quebec platform (Montreal, CA).

RNA-Seq data analysis

Raw reads were first filtered with Trimmomatic v0.38 with a minimum length (60 bp)[58], minimum quality (leading: 20; trailing: 20), and the presence of putative contaminants and remaining adaptors. Read quality was assessed before and after trimming with FastQC v0.11.8 and MultiQC v1.6[59]. Only high-quality paired-end reads were retained and mapped against the reference genome[60] using GSNAP v2018.07.04 with default parameters[61] but allowing a minimum mismatch value of 2 and a minimum read coverage of 90%. We used only properly paired and uniquely mapped reads for the downstream analysis[61].

The *KOGMWU* package[62] was used to test for rank-based enrichment of euKaryotic Orthologous Groups (KOG) and Gene Ontology (GO) terms using EggNOG-mapper v2.0[63] in the mantle, hemocytes and pearl sac sequencing datasets. The KOG_MWU function calculates delta rank values for these 23 broad functional groups using gene-level log2-fold changes (log2FC) generated from pairwise comparisons between MNP conditions and the control in the *DESeq2* v1.22.2 R package[64]. Transcriptomic responses to 0.025 and 1 µg L^{-1} MNPs were compared according to sample type to identify common and divergent patterns. Supplementary comparisons were performed between sample types for each MNP condition to identify common responses among tissue samples.

Weighted gene coexpression network analysis (WGCNA), implemented in R (v4.1.2) and based on VST (variance-stabilization) data values, was used to identify modules of genes whose expression

significantly correlated with conditions (control, 0.025 and 1 µg L^{-1}), MNP conditions (0.025 and 1 µg L^{-1}) and physiological and functional traits associated with the same individuals. A signed network was constructed using a soft threshold power of 13, a minimum module size of 50, and a module merging threshold of 25% dissimilarity. Module–trait relationships were computed by Pearson's correlation tests, and the correlated values were displayed within a heatmap, with $P < 0.05$ defined as indicating a significant correlation. Modules exhibiting a correlation ≥ 0.45 with $P \leq 0.01$ were selected as modules of interest. Eigengene expression within each module was also statistically analyzed to identify significant differences between conditions. GO enrichment analysis for BP and MF was performed on module genes using the Mann–Whitney *U* test implemented in the GOMWU framework using module kME input file, *P. margaritifera* annotations, *go.obo* database and a custom Perl script.

Differentially expressed genes (DEGs) were identified using HTSEQ v0.11.2[65]. The *DESeq2* package was used to examine differential expression between MNP and control conditions using a series of pairwise contrasts and Wald's tests. Genes were considered differentially expressed when the absolute value of log2FC was > 2 and the false discovery rate (FDR) was < 0.01. DEG interactions with the WGCNA modules of interest were then overlapped to identify potential links with differences between conditions, as well as associated physiological and functional trait relationships.

Statistical analysis

Data are presented as the mean with the 95% confidence interval of the mean (mean ± 1.96 standard error), except for frequency distributions, where data are presented as the mean ± standard deviation. Normality and homoscedasticity were tested with Shapiro–Wilk and Levene's tests, respectively. Data expressed in relative values were previously transformed by the arcsine square root function. Mean values were compared using one-way ANOVA for each condition ($\alpha = 0.05$). Tukey's post hoc test was used to evaluate the significance of differences between the averages of each group. When the assumptions of normality and homogeneity of variance were not met, we used the nonparametric Kruskal–Wallis test to compare the means of each condition. Dunn's post hoc test was used for multiple comparisons and to evaluate the significance of differences between the averages of each group. Frequency distributions were analyzed using Pearson's chi-squared test to determine if a difference occurred between conditions. Fisher's exact test was then used to compare conditions using a 2 × 2 contingency table. The results were considered significant at $P \leq 0.05$. All analyses were performed in the statistics software RStudio v4.1.2.

Declarations

Data availability

Open-source software were used for RNA-seq analysis: Trimmomatic (v0.38) (https://www.ncbi.nlm.nih.gov/tools/vecscreen/univec/), FastQC (v0.11.8) (https://www.bioinformatics.babraham.ac.uk/projects/fastqc/), MultiQC (v1.6), GSNAP (v2018.07.04), EggNOG-mapper (v2.0), DESeq2 (v1.22.2), HTSEQ (v0.11.2) and R (v4.1.2). RNA-seq data were deposited

into the European Bioinformatics Institute–European Nucleotide Archive (EBI–ENA) databank under the project ID PRJEB63073. Other data are included in the Supplementary Information file, as well as raw data for Figs. 1–2 and Supplementary Fig. 9 provided as a Source Data file with this article. Complementary information is available from the corresponding author on reasonable request.

Acknowledgements

The authors thank L. Bish of Ifremer (F-98719 Taravao, Tahiti, French Polynesia) for supplying microalgae during the 5-month experiment. We also thank G. Duflos, C. Himber and M. Colin from Anses, M. Kazour from the LOG and K. Mahé from Ifremer for participation in keshi pearl analyses. We are grateful to the Ifremer Bioinformatics Core Facility (SeBiMER; https://ifremer-bioinformatics.github.io/) for providing technical help and scientific support for bioinformatics analysis. The authors acknowledge the *Pôle de Calcul et de Données Marines* (PCDM; https://wwz.ifremer.fr/en/Research-Technology/Research-Infrastructures/Digital-infrastructures/Computation-Centre) for providing DATARMOR computing support and storage resources. The present study was supported by the MICROLAG project funded by the French Polynesian government under *Direction des Ressources Marines* (to T.G.), by a doctoral research grant No. 09793 from Ifremer (to T.G.), and by the European Union, the European Regional Development Fund (ERDF), the French State, the French Region Hauts-de-France and Ifremer under the framework of the project CPER MARCO 2015–2020 (to A.D.).

Author contributions

Conceptualization: T.G., G.L.M., A.H. Methodology: T.G., J.L.L., G.L.M., C.S., F.L., I.P.P., A.H. Investigation: T.G., J.L.L., C.S., F.L., A.D. Visualization: T.G. Supervision: T.G., J.L.L., G.L.M., A.H. Writing–original draft: T.G., J.L.L., A.D., I.P.P., A.H. Writing–review and editing: T.G., J.L.L., A.D., I.P.P., A.H.

Competing interests

The authors declare that they have no competing interests.

References

1. Lebreton, L. & Andrady, A. Future scenarios of global plastic waste generation and disposal. *Palgrave Commun.* **5,** 6 (2019).
2. Thompson, R. C. et al. Lost at sea: where is all the plastic? *Science* **304,** 838 (2004).
3. Andrady, A. L. Microplastics in the marine environment. *Mar. Pollut. Bull.* **62,** 1596-1605 (2011).
4. Eriksen, M. et al. Plastic pollution in the world's oceans: more than 5 trillion plastic pieces weighing over 250,000 tons afloat at sea. *PLoS One* **9,** e111913 (2014).
5. Rochman, C. M. et al. The ecological impacts of marine debris: unraveling the demonstrated evidence from what is perceived. *Ecology* **97,** 302-312 (2016).

6. Galloway, T. S., Cole, M. & Lewis, C. Interactions of microplastic debris throughout the marine ecosystem. *Nat. Ecol. Evol.* **1,** 116 (2017).
7. Sussarellu, R. et al. Oyster reproduction is affected by exposure to polystyrene microplastics. *Proc. Natl. Acad. Sci. U. S. A.* **113,** 2430-2435 (2016).
8. Gardon, T., Reisser, C., Soyez, C., Quillien, V. & Le Moullac, G. Microplastics affect energy balance and gametogenesis in the pearl oyster *Pinctada margaritifera*. *Environ. Sci. Technol.* **52,** 5277-5286 (2018).
9. Leslie, H. A., Brandsma, S. H., Van Velzen, M. J. & Vethaak, A. D. Microplastics en route: field measurements in the Dutch river delta and Amsterdam canals, wastewater treatment plants, North Sea sediments and biota. *Environ. Int.* **101,** 133-142 (2017).
10. Bessa, F. et al. Occurrence of microplastics in commercial fish from a natural estuarine environment. *Mar. Pollut. Bull.* **128,** 575-584 (2018).
11. Watts, A. J. et al. Effect of microplastic on the gills of the shore crab *Carcinus maenas*. *Environ. Sci. Technol.* **50,** 5364-5369 (2016).
12. Cole, M., Lindeque, P., Fileman, E., Halsband, C. & Galloway, T. S. The impact of polystyrene microplastics on feeding, function and fecundity in the marine copepod *Calanus helgolandicus*. *Environ. Sci. Technol.* **49,** 1130-1137 (2015).
13. Watts, A. J., Urbina, M. A., Corr, S., Lewis, C. & Galloway, T. S. Ingestion of plastic microfibers by the crab *Carcinus maenas* and its effect on food consumption and energy balance. *Environ. Sci. Technol.* **49,** 14597-14604 (2015).
14. Phuong, N. N. et al. Is there any consistency between the microplastics found in the field and those used in laboratory experiments? *Environ. Pollut.* **211,** 111-123 (2016).
15. Lenz, R., Enders, K. & Nielsen, T. G. Microplastic exposure studies should be environmentally realistic. *Proc. Natl. Acad. Sci. U. S. A.* **113,** E4121-E4122 (2016).
16. Paul-Pont, I. et al. Constraints and priorities for conducting experimental exposures of marine organisms to microplastics. *Front. Mar. Sci.* **5,** 252 (2018).
17. Revel, M. et al. Tissue-specific biomarker responses in the blue mussel *Mytilus* spp. exposed to a mixture of microplastics at environmentally relevant concentrations. *Front. Environ. Sci.* **7,** 33 (2019).
18. Pannetier, P. et al. Environmental samples of microplastics induce significant toxic effects in fish larvae. *Environ. Int.* **134,** 105047 (2020).
19. Schür, C., Zipp, S., Thalau, T. & Wagner, M. Microplastics but not natural particles induce multigenerational effects in *Daphnia magna*. *Environ. Pollut.* **260,** 113904 (2020).
20. Koelmans, A. A. et al. Risks of plastic debris: unravelling fact, opinion, perception, and belief. *Environ. Sci. Technol.* **51,** 11513-11519 (2017).
21. Siu, D. *Les Exportations de Produits Perliers, Fortement Impactées par la Covid-19 en 2020* (ISPF, French Polynesia, 2021).

22. Andréfouët, S., Thomas, Y. & Lo, C. Amount and type of derelict gear from the declining black pearl oyster aquaculture in Ahe atoll lagoon, French Polynesia. *Mar. Pollut. Bull.* **83,** 224-230 (2014).
23. Gardon, T. et al. Microplastics contamination in pearl-farming lagoons of French Polynesia. *J. Hazard. Mater.* **419,** 126396 (2021).
24. Gardon, T. et al. Microplastics induce dose-specific transcriptomic disruptions in energy metabolism and immunity of the pearl oyster *Pinctada margaritifera*. *Environ. Pollut.* **266,** 115180 (2020).
25. Albentosa, M., Viñas, L., Besada, V., Franco, A. & González-Quijano, A. First measurements of the scope for growth (SFG) in mussels from a large scale survey in the North-Atlantic Spanish coast. *Sci. Total Environ.* **435-436,** 430-445 (2012).
26. Hawkins, A., James, M., Hickman, R., Hatton, S. & Weatherhead, M. Modelling of suspension-feeding and growth in the green-lipped mussel *Perna canaliculus* exposed to natural and experimental variations of seston availability in the Marlborough Sounds, New Zealand. *Mar. Ecol. Prog. Ser.* **191,** 217-232 (1999).
27. Sokolova, I. M. Energy-limited tolerance to stress as a conceptual framework to integrate the effects of multiple stressors. *Integr. Comp. Biol.* **53,** 597-608 (2013).
28. Crawford, D. R., Wang, Y., Schools, G. P., Kochheiser, J. & Davies, K. J. Down-regulation of mammalian mitochondrial RNAs during oxidative stress. *Free Radic. Biol. Med.* **22,** 551-559 (1997).
29. Zhang, W. & Liu, H. T. MAPK signal pathways in the regulation of cell proliferation in mammalian cells. *Cell Res.* **12,** 9-18 (2002).
30. Jeong, C. B. et al. Adverse effects of microplastics and oxidative stress-induced MAPK/Nrf2 pathway-mediated defense mechanisms in the marine copepod *Paracyclopina nana*. *Sci. Rep.* **7,** 41323 (2017).
31. Udensi, U. K. & Tchounwou, P. B. Potassium homeostasis, oxidative stress, and human disease. *Int. J. Clin. Exp. Physiol.* **4,** 111-122 (2017).
32. Ni, K. D. & Liu, J. Y. The functions of cytochrome P450 ω-hydroxylases and the associated eicosanoids in inflammation-related diseases. *Front. Pharmacol.* **12,** 716801 (2021).
33. Tan, H., Yue, T., Xu, Y., Zhao, J. & Xing, B. Microplastics reduce lipid digestion in simulated human gastrointestinal system. *Environ. Sci. Technol.* **54,** 12285-12294 (2020).
34. Shang, Y. et al. The effect of microplastics on the bioenergetics of the mussel *Mytilus coruscus* assessed by cellular energy allocation approach. *Front. Mar. Sci.* **8,** 754789 (2021).
35. Kültz, D. Molecular and evolutionary basis of the cellular stress response. *Annu. Rev. Physiol.* **67,** 225-257 (2005).
36. Pott, D. M., Osorio, S. & Vallarino, J. G. From central to specialized metabolism: an overview of some secondary compounds derived from the primary metabolism for their role in conferring nutritional and organoleptic characteristics to fruit. *Front. Plant Sci.* **10,** 835 (2019).
37. Torres, J. P. & Schmidt, E. W. The biosynthetic diversity of the animal world. *J. Biol. Chem.* **294,** 17684-17692 (2019).

38. Chomel, M. et al. Plant secondary metabolites: a key driver of litter decomposition and soil nutrient cycling. *J. Ecol.* **104,** 1527-1541 (2016).
39. Kim, S. W., Liang, Y., Lozano, Y. M. & Rillig, M. C. Microplastics reduce the negative effects of litter-derived plant secondary metabolites on nematodes in soil. *Front. Environ. Sci.* **9,** 790560 (2021).
40. Forbey, J. S. et al. Exploitation of secondary metabolites by animals: a response to homeostatic challenges. *Integr. Comp. Biol.* **49,** 314-328 (2009).
41. Muhammad, G., Atsumi, T., Sunardi & Komaru, A. Nacre growth and thickness of Akoya pearls from Japanese and Hybrid *Pinctada fucata* in response to the aquaculture temperature condition in Ago Bay, Japan. *Aquaculture* **477,** 35-42 (2017).
42. Joubert, C. et al. Temperature and food influence shell growth and mantle gene expression of shell matrix proteins in the pearl oyster *Pinctada margaritifera*. *PLoS One* **9,** e103944 (2014).
43. Le Pabic, L. et al. Culture site dependence on pearl size realization in *Pinctada margaritifera* in relation to recipient oyster growth and mantle graft biomineralization gene expression using the same donor phenotype. *Estuar. Coast. Shelf Sci.* **182,** 294-303 (2016).
44. Al-Sid-Cheikh, M. et al. Uptake, whole-body distribution, and depuration of nanoplastics by the scallop *Pecten maximus* at environmentally realistic concentrations. *Environ. Sci. Technol.* **52,** 14480-14486 (2018).
45. Han, Z., Jiang, T., Xie, L. & Zhang, R. Microplastics impact shell and pearl biomineralization of the pearl oyster *Pinctada fucata*. *Environ. Pollut.* **293,** 118522 (2021).
46. Cominassi, L. et al. Food availability modulates the combined effects of ocean acidification and warming on fish growth. *Sci. Rep.* **10,** 2338 (2020).
47. Wen, B. et al. Microplastics have a more profound impact than elevated temperatures on the predatory performance, digestion and energy metabolism of an Amazonian cichlid. *Aquat. Toxicol.* **195,** 67-76 (2018).
48. Gardon, T. et al. Cryogrinding and sieving techniques as challenges towards producing controlled size range microplastics for relevant ecotoxicological tests. *Environ. Pollut.* **315,** 120383 (2022).
49. Pouvreau, S., Jonquières, G. & Buestel, D. Filtration by the pearl oyster, *Pinctada margaritifera*, under conditions of low seston load and small particle size in a tropical lagoon habitat. *Aquaculture* **176,** 295-314 (1999).
50. Linard, C. et al. Calcein staining of calcified structures in pearl oyster *Pinctada margaritifera* and the effect of food resource level on shell growth. *Aquaculture* **313,** 149-155 (2011).
51. Khosrovyan, A. & Kahru, A. Virgin and UV-weathered polyamide microplastics posed no effect on the survival and reproduction of *Daphnia magna*. *PeerJ* **10,** e13533 (2022).
52. Gueguen, Y. et al. Yes, it turns: experimental evidence of pearl rotation during its formation. *R. Soc. Open Sci.* **2,** 150144 (2015).
53. Chávez-Villalba, J., Soyez, C., Aurentz, H. & Le Moullac, G. Physiological responses of female and male black-lip pearl oysters (*Pinctada margaritifera*) to different temperatures and concentrations of

food. *Aquat. Living Resour.* **26,** 263-271 (2013).

54. Savina, M. & Pouvreau, S. A comparative ecophysiological study of two infaunal filter-feeding bivalves: *Paphia rhomboïdes* and *Glycymeris glycymeris*. *Aquaculture* **239,** 289-306 (2004).
55. Bayne, B. L., Hawkins, A. J. S. & Navarro, E. Feeding and digestion by the mussel *Mytilus edulis* L. (Bivalvia: Mollusca) in mixtures of silt and algal cells at low concentrations. *J. Exp. Mar. Biol. Ecol.* **111,** 1-22 (1987).
56. Hermabessiere, L. et al. Optimization, performance, and application of a pyrolysis-GC/MS method for the identification of microplastics. *Anal. Bioanal. Chem.* **410,** 6663-6676 (2018).
57. Djouina, M. et al. Oral exposure to polyethylene microplastics alters gut morphology, immune response, and microbiota composition in mice. *Environ. Res.* **212,** 113230 (2022).
58. Bolger, A. M., Lohse, M. & Usadel, B. Trimmomatic: a flexible trimmer for Illumina sequence data. *Bioinformatics* **30,** 2114-2120 (2014).
59. Ewels, P., Magnusson, M., Lundin, S. & Käller, M. MultiQC: summarize analysis results for multiple tools and samples in a single report. *Bioinformatics* **32,** 3047-3048 (2016).
60. Le Luyer, J. et al. Whole transcriptome sequencing and biomineralization gene architecture associated with cultured pearl quality traits in the pearl oyster, *Pinctada margaritifera*. *BMC Genom.* **20,** 111 (2019).
61. Wu, T. D., Reeder, J., Lawrence, M., Becker, G. & Brauer, M. J. GMAP and GSNAP for genomic sequence alignment: enhancements to speed, accuracy, and functionality in *Statistical Genomics: Methods and Protocols* (eds Mathé, E., Davis, S.) 283-334. (Springer, New York, NY, 2016).
62. Dixon, G. B. et al. Genomic determinants of coral heat tolerance across latitudes. *Science* **348,** 1460-1462 (2015).
63. Huerta-Cepas, J. et al. Fast genome-wide functional annotation through orthology assignment by eggNOG-mapper. *Mol. Biol. Evol.* **34,** 2115-2122 (2017).
64. Love, M. I., Huber, W. & Anders, S. Moderated estimation of fold change and dispersion for RNA-seq data with DESeq2. *Genome Biol.* **15,** 550 (2014).
65. Anders, S., Pyl, P. T. & Huber, W. HTSeq–a Python framework to work with high-throughput sequencing data. *Bioinformatics* **31,** 166-169 (2015).

Figures

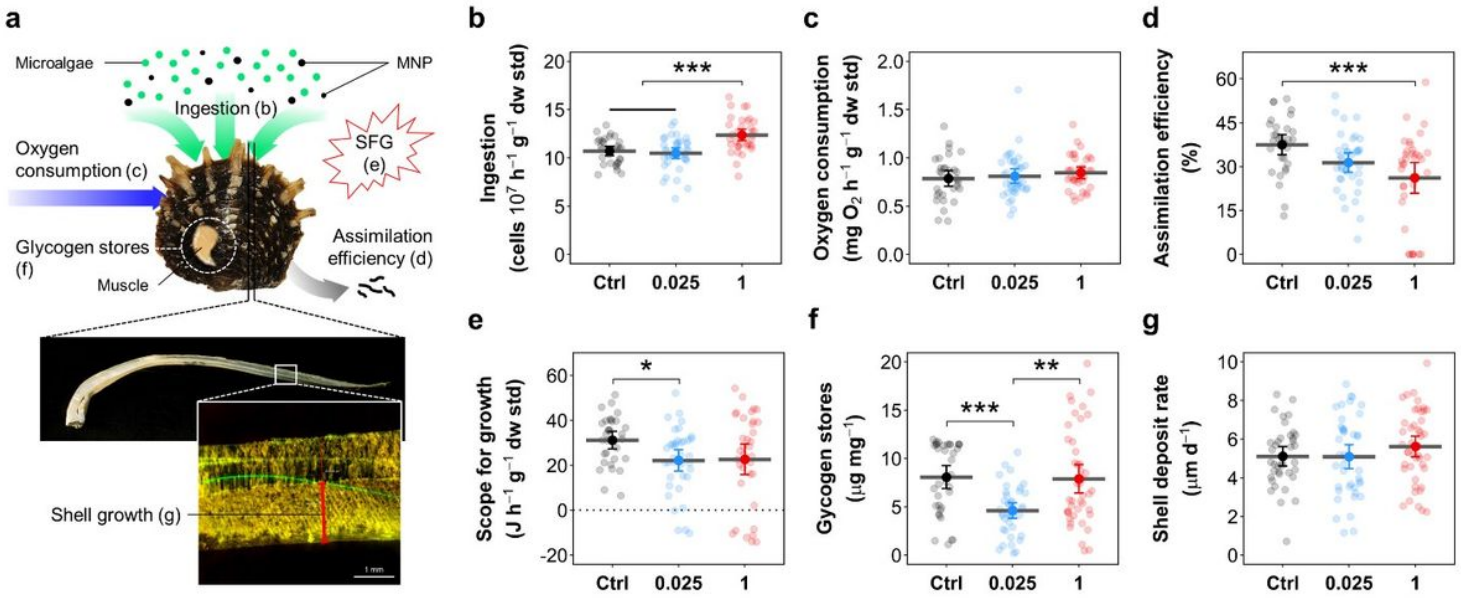

Figure 1

Physiological parameters of *P. margaritifera* exposed to micro-nanoplastics. (**a**) Schematic of the monitored ecophysiological parameters. (**b-g**) Boxplots showing the effect of MNP exposure on (**b**) ingestion rate, (**c**) oxygen consumption, (**d**) assimilation efficiency, (**e**) scope for growth (SFG), (**f**) glycogen stores and (**g**) shell growth. Data are expressed as the mean with the 95% confidence interval ($31 \leq N \leq 46$). Asterisks indicate statistically significant differences between conditions ("*", $P < 0.05$; "**", $P < 0.01$; "***", $P < 0.001$).

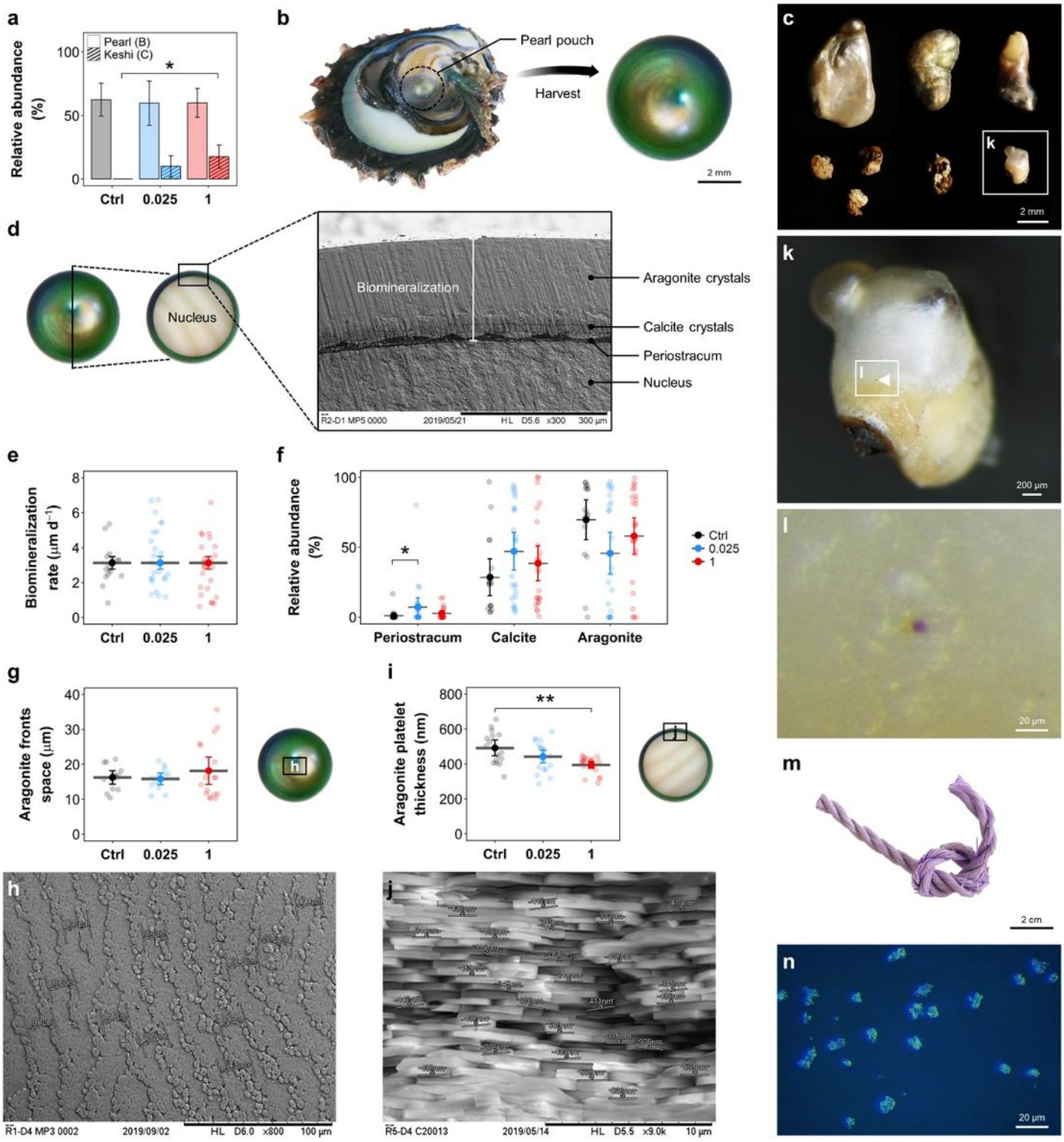

Figure 2

Functional results following a 3-month pearl production cycle under micro-nanoplastics exposure. (**a**) Histograms of the frequency distribution of collected (**b**) pearls and (**c**) keshi pearls showing different morphotypes. Pearl quality assessment was based on (**d**) biomineral secretion produced on the nucleus for 3 months, which was used to obtain (**e**) the biomineralization rate and (**f**) the relative abundance of pearl nacre deposition structures composed of periostracum, calcite and aragonite crystals. The

aragonite crystal microstructure was also characterized according to the aragonite (**g** and **h**) front space (the pearl surface) and (**i** and **j**) platelet thickness *via* SEM of pearl cross sections. (**k** and **l**) Observation of a particle with a purple color identified in the mineral surface microlayer of a keshi pearl. (**m** and **n**) Pictures of the weathered purple synthetic rope used to produce PE micro-nanoplastics in the present study. Data are expressed as the mean with the 95% confidence interval of the mean ($17 \leq N \leq 25$), except for **a**, which shows the mean ± standard deviation. Asterisks indicate statistically significant differences between conditions ("*", $P < 0.05$; "**", $P < 0.01$).

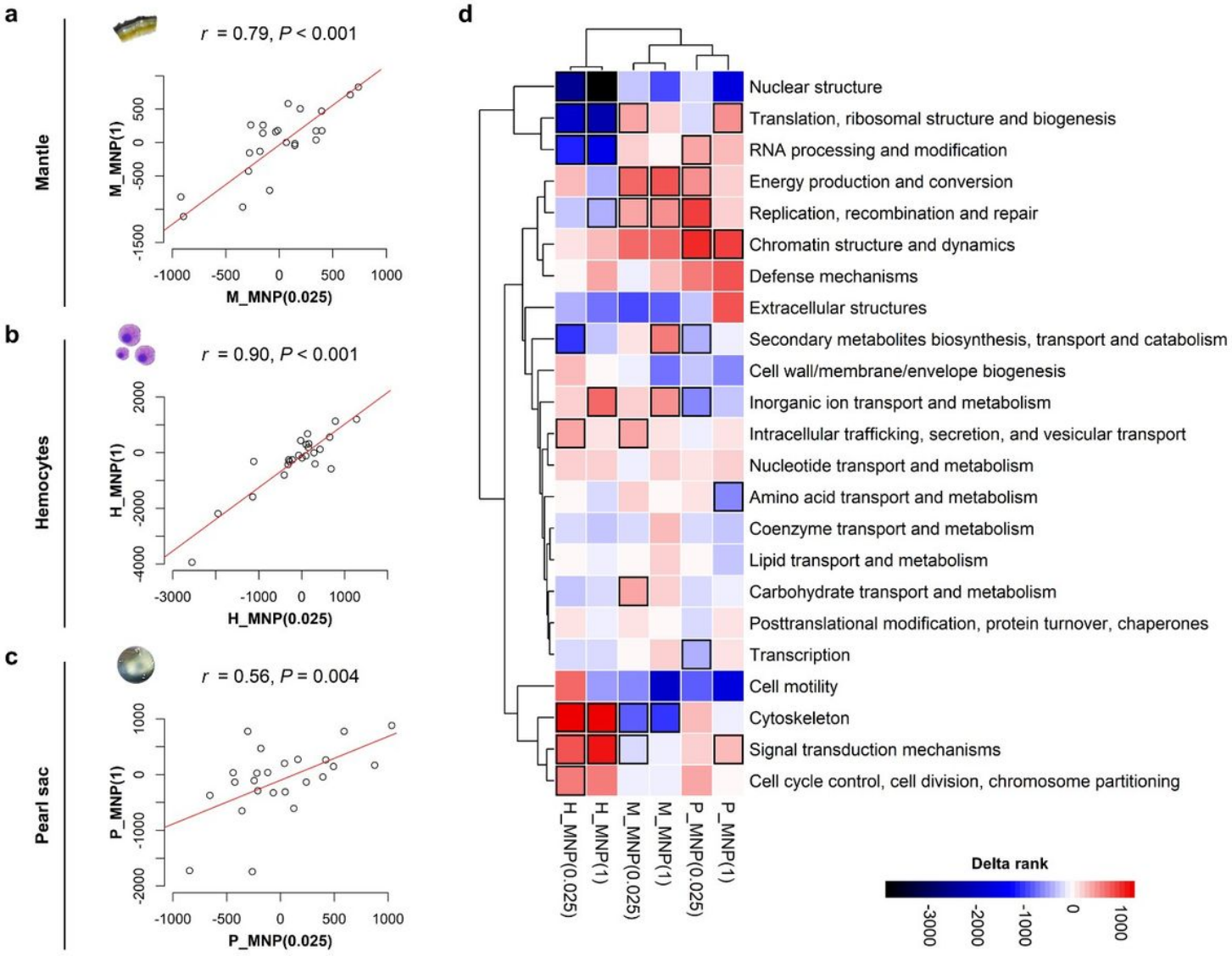

Figure 3

Hierarchical clustering analysis of KOG enrichments in the *P. margaritifera* transcriptome following micro-nanoplastics exposure. Pearson's correlations of KOG delta rank values in the (**a**) mantle, (**b**) hemocytes and (**c**) pearl sac of *P. margaritifera* exposed to 0.025 and 1 µg MNPs L^{-1}. (**d**) Shared KOG term enrichments (rows) among up- or downregulated genes (delta rank heatmap) under MNP conditions

across tissues (columns; M: mantle, H: hemocytes or P: pearl sac). KOG categories in bolded squares denote statistically significant enrichments (FDR-adjusted $P < 0.05$).

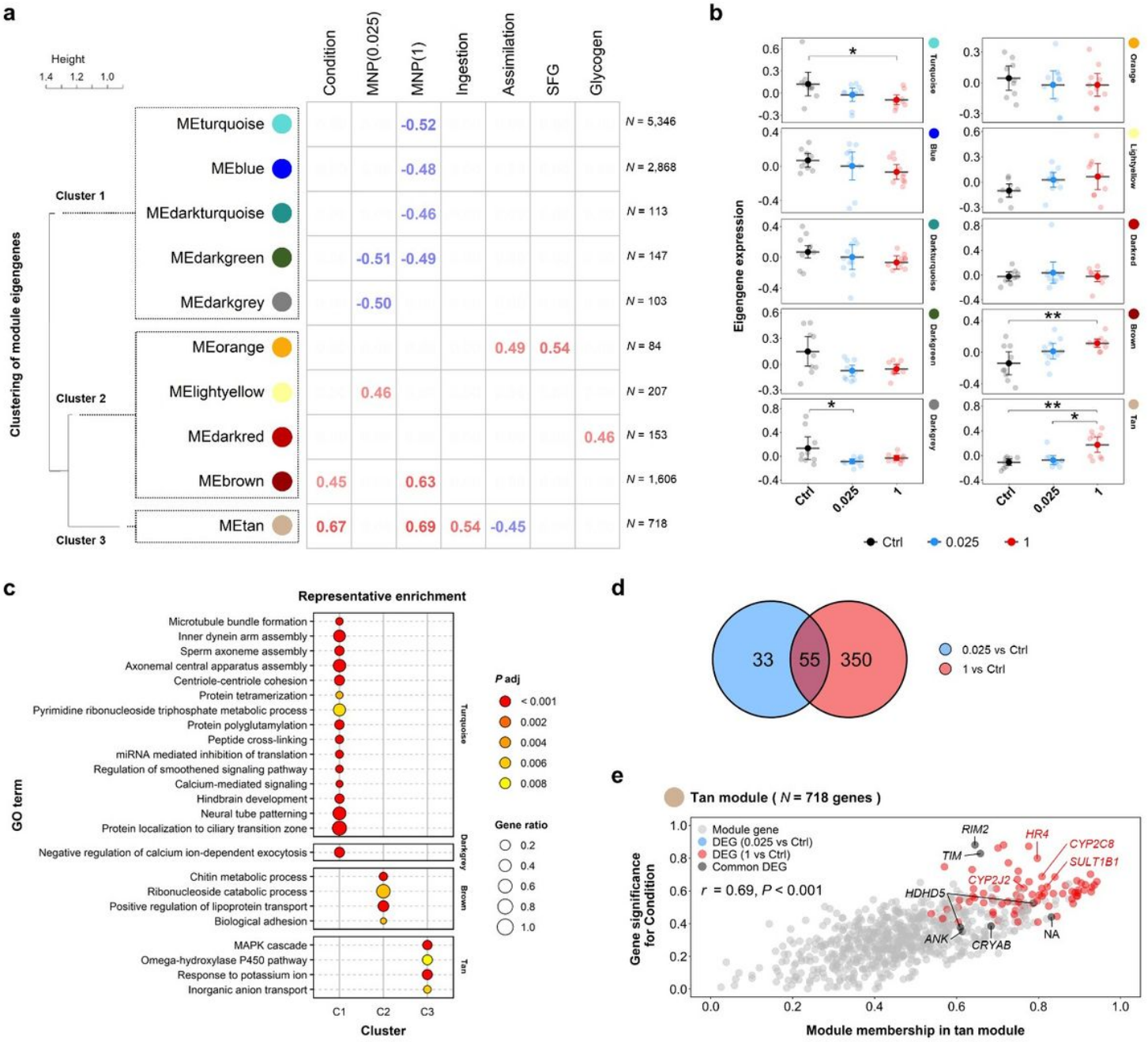

Figure 4

Transcriptomic responses in the mantle of *P. margaritifera* after a 5-month exposure to micro-nanoplastics. (**a**) Heatmap of identified modules (*y*-axis) and functionally enriched pathways in relation to experimental traits ($|r| \geq 0.45$, $P \leq 0.01$; *x*-axis) from WGCNA. The clustering tree of module eigengenes (MEs) on the left is based on a merging threshold of 100% dissimilarity initially established at 25% for network construction. The numbers on the right of the heatmap represent the number of genes identified in each module. (**b**) Eigengene expression for selected WGCNA modules significantly correlated with

experimental conditions and/or physiological traits in response to MNP exposure ("*", $P < 0.05$; "**", $P < 0.01$). Data are expressed as the mean with the 95% confidence interval ($N = 9–10$). (**c**) Representative functional enrichment analysis of module genes identified in the turquoise, darkgrey, brown and tan modules based on an adjusted P value cutoff ($P < 0.01$) and cut-height (0.8) of the GO terms tree to obtain "independent groups". The dendrograms depict the sharing of genes between categories; the fractions correspond to genes with $P < 0.05$ relative to the total number of genes within the category. (**d**) Venn diagram of differentially expressed genes (DEGs) in both MNP conditions compared to the control (|log2FC| > 2; FDR < 0.01). (**e**) Scatterplot of gene significance for condition *vs.* module membership in the tan module illustrating module-trait associations. Gray genes represent module genes; blue and red genes represent DEGs specific to 0.025 and 1 µg L^{-1} MNPs, respectively, with labeled red genes ($N = 4$) identified as common DEGs with other tissues (hemocytes and pearl sac) in the 1 µg L^{-1} condition, including *CYP2J2* and *CYP2C8* (cytochrome P450 family 2 subfamily J member 2 and subfamily C member 8, respectively), *HR4* (hormone receptor 4) and *SULT1B1* (sulfotransferase family 1B member 1); labeled black genes represent common DEGs in both MNP conditions ($N = 7$, of which 6 were annotated), including 2 transcript variants of *HDHD5* (haloacid dehalogenase-like hydrolase domain containing 5), *RIM2* (replication in mitochondria 2), *CRYAB* (crystallin alpha B), *TIM* (timeless) and *ANK* (ankyrin).

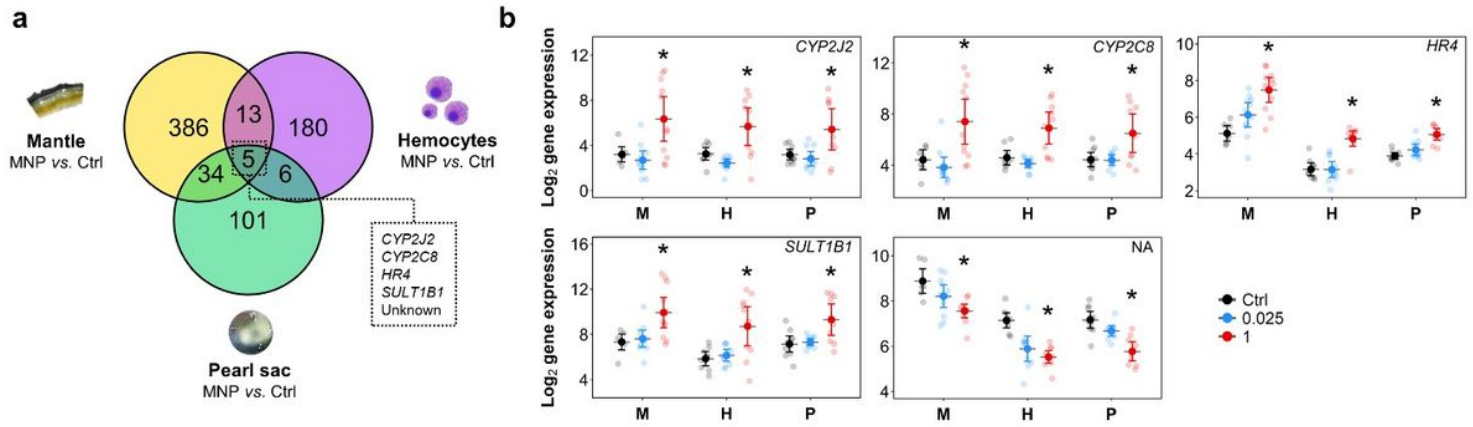

Figure 5

Differentially expressed genes across *P. margaritifera* tissues after a 5-month exposure to micro-nanoplastics. (**a**) Venn diagram of shared differentially expressed genes (DEGs) in mantle, hemocyte and pearl sac samples identified in both MNP conditions compared to the control (|log2FC| > 2; FDR < 0.01). (**b**) Boxplots of gene expression associated with DEGs common to the tissue samples, including *CYP2J2* and *CYP2C8*(cytochrome P450 family 2 subfamily J member 2 and subfamily C member 8, respectively), *HR4*(hormone receptor 4), *SULT1B1* (sulfotransferase family 1B member 1) and an unannotated gene (NA). Significant differences between the control and MNP conditions (|log2FC| > 2; FDR < 0.01) are represented by an asterisk ("*"). Data are expressed as the mean with the 95% confidence interval ($7 \leq N \leq 12$). M: mantle; H: hemocytes; P: pearl sac.

Supplementary Files

This is a list of supplementary files associated with this preprint. Click to download.

- SourceDataGardonetal.xlsx
- SupplementaryInformationGardonetal.docx